Downloaded from rsta.royalsocietypublishing.org

PHILOSOPHICAL TRANSACTIONS OF THE ROYAL SOCIETY A MATHEMATICAL, PHYSICAL & ENGINEERING SCIENCES

Observations of the Structure of the Upper Ocean: Wind-Driven Momentum Budget

R. T. Pollard

Phil. Trans. R. Soc. Lond. A 1983 **308**, 407-425
doi: 10.1098/rsta.1983.0012

Email alerting service

Receive free email alerts when new articles cite this article - sign up in the box at the top right-hand corner of the article or click **here**

To subscribe to *Phil. Trans. R. Soc. Lond. A* go to: **http://rsta.royalsocietypublishing.org/subscriptions**

This journal is © 1983 The Royal Society

Downloaded from rsta.royalsocietypublishing.org

Phil. Trans. R. Soc. Lond. A **380**, 407–425 (1983)
Printed in Great Britain

Observations of the structure of the upper ocean: wind-driven momentum budget

By R. T. Pollard

Institute of Oceanographic Sciences, Brook Road, Wormley, Godalming, Surrey, GU8 5UB, U.K.

The response of the surface layer to a sudden 0.3 N m^{-2} wind event is described in unusual detail by combining current data from instruments hung beneath a drifting spar buoy with temperature and salinity data from conductivity–temperature–depth sensors on an undulating vehicle towed 26 times around a square of side 7 km, maintaining position relative to the drifting spar. Horizontal advection is minimized by the Lagrangian experiment.

The momentum equations for the wind-driven response of the surface layer cannot be balanced by wind stress, temporal rate of change and coriolis terms alone. Mixing rearranges vertical and horizontal density gradients, resulting in a mixed-layer depth that slopes horizontally at about 10^{-3} (1 m km^{-1}), which in turn modifies pressure gradient terms, causing thermal wind shear across the base of the mixing layer of up to 1 cm s^{-1} m^{-1}. Rapid adjustment of the pressure gradient terms is the most probable cause of inertial oscillations 50 % larger than can be accounted for by wind stress alone, but tidal–inertial interactions are also significant. The geostrophic, wind-driven mean and inertial currents are depth independent within 2 cm s^{-1} in the mixing layer, at least from the shallowest current meter at 14 down to 25 m.

1. Introduction

This paper describes a single case study of the development of the mixing layer spanning only a few days. The study was one of several undertaken as contributions to the Joint Air–Sea Interaction experiment JASIN 1978 (Pollard *et al.* this symposium). The structure found is complex, and should be considered in the light of the eddy (Ellett *et al.* this symposium; Pollard 1982*a*) and frontal (Minnett *et al.* this symposium; Pollard 1982*b*) structures that were also present in the JASIN area. Indeed one of the main strengths of JASIN was that it provided the synoptic context within which case studies such as this one should ideally always be placed.

To draw any conclusions, frequent cross-referencing and intercomparison of data from several different sources is necessary. To familiarize the reader with the data sets under consideration, instrumentation and data reduction are first described in §2, which ends with an introduction to the response of the system to the wind event to be analysed. The momentum balance averaged over an inertial period is then discussed in §3 and the time-varying momentum balance (the inertial oscillations) in §4. The main observations and conclusions are summarized in §5.

2. Instrumentation and data reduction

Drifting spar and navigation

The focus of the experiment was a free-drifting spar buoy supporting vector-averaging instruments to measure velocity and temperature at depths between 14 and 42 m (figure 1*a*). With such a configuration, it was hoped to (*a*) minimize wave noise in the current measurements,

The Royal Society is collaborating with JSTOR to digitize, preserve, and extend access to *Philosophical Transactions of the Royal Society of London. Series A, Mathematical and Physical Sciences.* www.jstor.org

Downloaded from rsta.royalsocietypublishing.org

(*b*) minimize drag moments tending to tilt the spar, and (*c*) minimize windage so that the spar would drift with the mean velocity of the mixing layer.

The underwater cross-section of the 8.9 m long, 0.25 m diameter spar, including a 0.5 m diameter canvas sleeve covering the bottom 3.0 m, was 3.14 m^2, compared with 2.67 m^2 for all instruments. Although the 2.0 m long, 0.11 m diameter surface-piercing section of the spar had only 0.12 m^2 cross-section to the wind, the spar had to be tethered to an uninstrumented pitch–roll buoy to provide backup buoyancy, itself tethered to a dan buoy with radar reflector for navigation and location. Thus some windage was inevitable, and will be shown to be about 0.1 $m\,s^{-1}$ for a 15 $m\,s^{-1}$ wind. The natural heave period of oscillation of the instrumented spar was calculated to be 25.6 s.

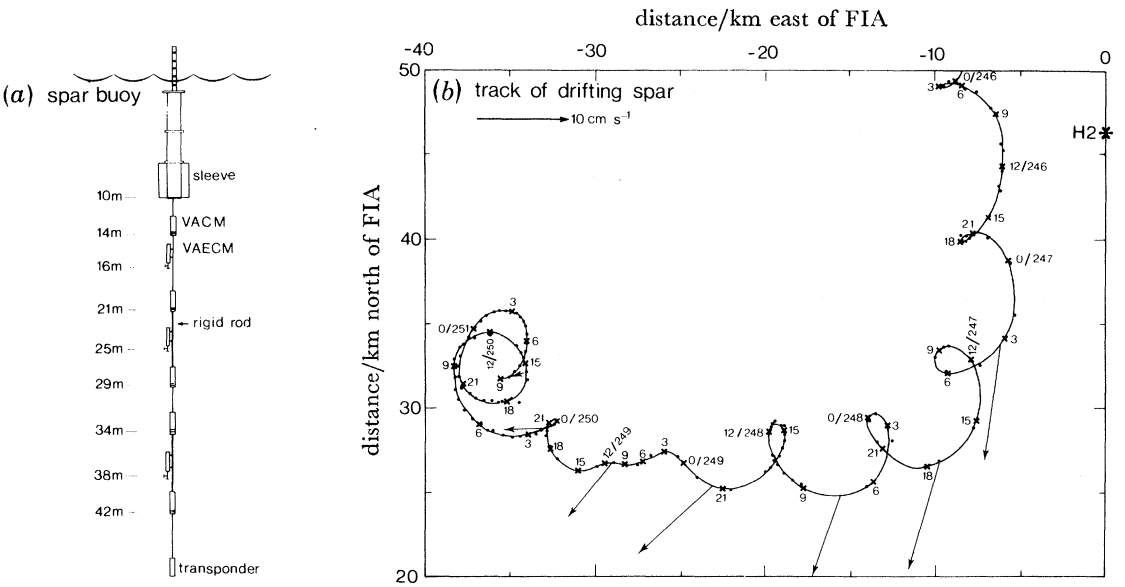

FIGURE 1. (*a*) Schematic of the drifting spar showing the depths of vector-averaging (VACM) and open-head electromagnetic (VAECM) current meters. (*b*) Loran C position fixes (dots) on the drifting spar have been fitted by a cubic spline with knots every three hours. Hour (G.M.T.)/day number is marked every three hours (crosses). The r.m.s. distance between observed and calculated positions is 90 m. Fourteen-hour mean absolute velocities at 42 m are also shown (arrows). Mooring H2 (asterisk) was recovered at 1500/246. (FIA, fixed intensive array.)

Five of the current meters were standard AMF vector-averaging current meters (VACMS) with 112.5 s averaging periods measuring horizontal velocity and temperature. The remaining three were electromagnetic vector-averaging current meters (VAECMS), designed and built at the Institute of Oceanographic Sciences. Each carried two open-head toroidal electromagnetic coils, intended to measure three components of velocity, though only the horizontal velocity will be discussed here. Unfortunately two of the VAECM compasses (those at 16 and 25 m) had been supplied with faulty bearings, which caused a sluggish directional response which is apparent in the data. However, in the rough conditions to be described, wave action prevents the compass from seizing up completely. While the data must be regarded with caution, they still contain usable information, and are included in this paper.

The track of the drifting spar relative to ground (figure 1*b*) was determined in several stages. If the tending ship, R.R.S. *Discovery*, was on station, the range of the spar from the ship was measured acoustically, with visual or radar bearing. If the ship was moving, improved accuracy was obtained by sampling acoustic range several times as the ship passed close by the spar. The

Downloaded from rsta.royalsocietypublishing.org

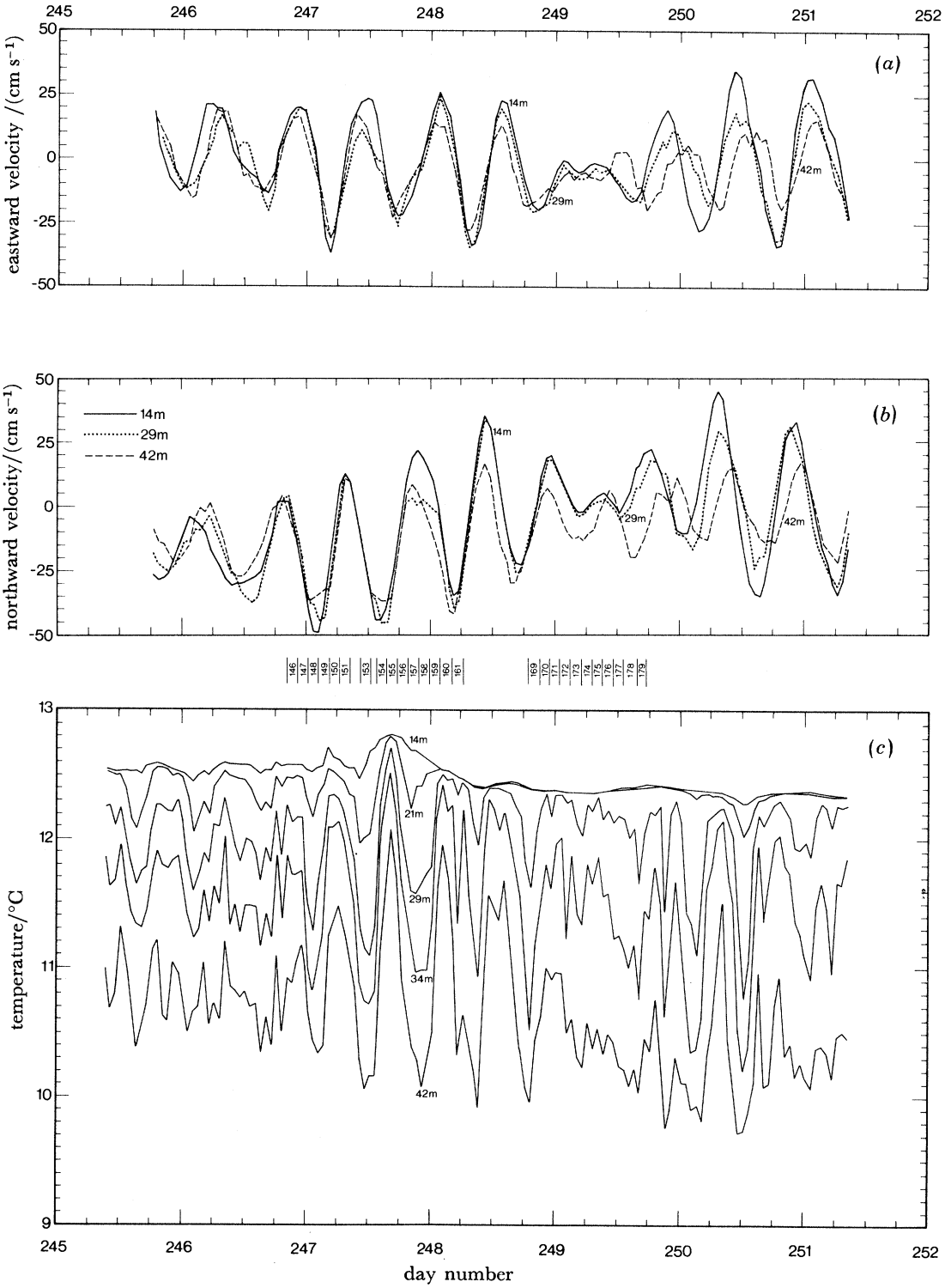

FIGURE 2. One-hour averaged time series of (*a*) eastward and (*b*) northward components of absolute velocity and of (*c*) temperature for selected VACMs. Absolute velocity is the vector sum of the current meter velocity (relative to the spar) and the absolute velocity of the drifting spar (from figure 1). The times of circuits 146 to 179 (figure 3) are also shown.

Downloaded from rsta.royalsocietypublishing.org

position of R.R.S. *Discovery* was determined by taking Loran C fixes averaged over a one-minute interval every thirty minutes. Positions between fixes were interpolated by using the two-component electromagnetic (EM) ship's log, a constant current being assumed. This method gave a smoother ship track plot than using Loran alone (Pollard & Saunders 1978*a*, *b*), and Loran gave significantly better fixes relative to the Loran grid (r.m.s. error about 200 m) than satellite fixes (error 400–1000 m).

Absolute spar positions were determined every half hour when R.R.S. *Discovery* was on station, but only every two hours when steaming. To obtain an hourly time series of spar positions, cubic splines were fitted separately to the x- and y-coordinates of the spar position fixes against time. Each spline segment was three hours long, and continuity of the functions $x(t)$, $y(t)$ and their first and second derivations was forced at each knot between segments.

Hourly absolute currents were determined by vector adding the absolute velocity of the spar to the current meter data relative to the spar (figures 2*a*, *b*), resolving tidal and inertial period oscillations, but averaging out higher frequency internal waves. The time series are dominated by tidal and inertial oscillations of amplitude up to 30 cm s^{-1}, superimposed on a mean flow that was initially 15 cm s^{-1} to the south (figure 1*b*).

The temperature sensors on the five VACMs were calibrated before and after the experiment with an accuracy of 10 mK, but, when two or more instruments were in a well mixed surface layer, occasional implausible inversions were observed, which were caused by calibration uncertainties. Since the VACMs were deployed seven times during the entire experiment (only one of which is described here) in different vertical configurations, it was possible to build up a consistent set of relative temperature corrections to minimize inversions. The corrections ranged from +10 to −10 mK (Pollard 1980*b*), and the corrected time series (figure 2*c*) are estimated to have a relative accuracy of 2 mK.

Towed conductivity–temperature–depth (CTD) data

After deploying the drifting spar, R.R.S. *Discovery* carried out repeated surveys of the upper 30–50 m of the water column, with a Neil Brown Instrument Systems' (N.B.I.S.) CTD mounted in an Institute of Oceanographic Sciences' Sea-Soar. The Sea-Soar, developed from the Hermes Batfish (Dessureault 1976), is towed behind the ship, undulating in the vertical in a sawtooth pattern controlled from the ship. The maximum and minimum depths, and the ascent and descent rates are all adjustable by using the Hermes Batfish control unit.

The survey consisted of repeated squares, with sides 7–8 km long, which could be completed in about two hours. The period was chosen to allow the mixing-layer development during a sudden wind event to be monitored. Starting 1 km south of the drifting spar, the ship steered due east, then due north, then due west, each for thirty minutes. The direction of the final, approximately southward, side was adjusted to pass 1 km west of the drifting spar, where the ship turned east to begin another circuit. Thus the spar is at the southwest corners of the Sea-Soar circuits (figure 3*a*), which are numbered 146 to 151, 153 to 162, and 169 to 179 (table 1).

To produce the track plot relative to ground (figure 3*a*), the ship's EM log data were combined with Loran C fixes as described above. By using the EM log data without Loran C correction, a track plot relative to water can be derived (figure 3*b*). The track is relative to water at a depth of 6 m, the depth of the EM sensor head. The relative distance scales on figure 3*b* can be interpreted as positions relative to the Fixed Intensive Array (FIA) (Pollard *et al.* this symposium)

PHILOSOPHICAL TRANSACTIONS OF THE ROYAL SOCIETY A MATHEMATICAL, PHYSICAL & ENGINEERING SCIENCES

PHILOSOPHICAL TRANSACTIONS OF THE ROYAL SOCIETY A MATHEMATICAL, PHYSICAL & ENGINEERING SCIENCES

Downloaded from rsta.royalsocietypublishing.org

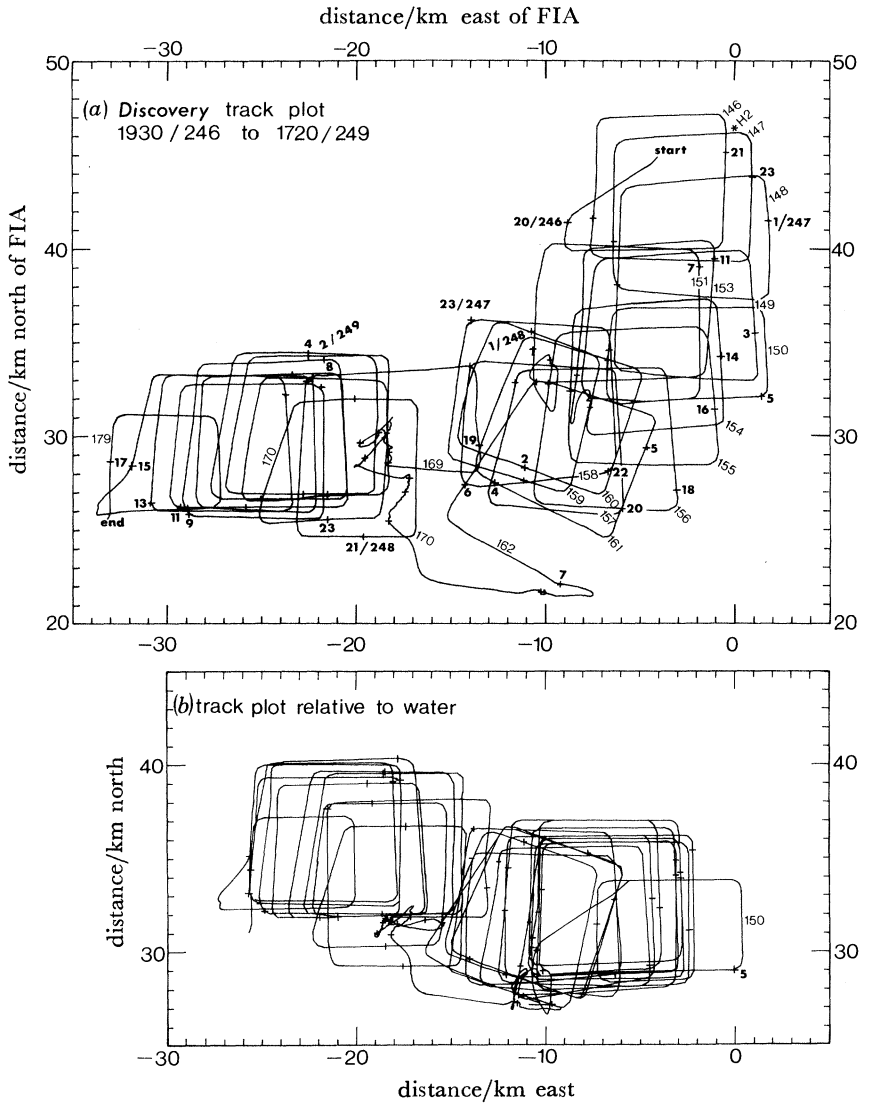

FIGURE 3. Ship track plots relative to (*a*) ground, (*b*) water. The relative plot is determined from the ship's two-component EM log situated below the hull at a depth of 6 m. Adjustment to absolute positions was by half-hourly Loran C observations. Hourly positions are shown (crosses) and some are labelled with hour or hour/day number (bold). Each 2 h circuit is numbered. Circuits are defined to start at the southwest corner of each square, where the ship turns east around the drifting spar, about 1 km off it (compare figure 1*b*). The western sides of circuits between 170 and 179 progress steadily westwards, and so have not been individually labelled.

TABLE 1. START TIMES (HOUR/DAY NUMBER) OF SEA-SOAR CIRCUITS

circuit	start	circuit	start	circuit	start	circuit	start
145	1933/246	153	1017/247	160	0141/248	173	0243/249
146	2010/246	154	1322/247	161	0358/248	174	0451/249
147	2208/246	155	1514/247	162	0608/248	175	0649/249
148	0008/247	156	1723/247	169	1835/248	176	0857/249
149	0217/247	157	1928/247	170	2042/248	177	1058/249
150	0419/247	158	2137/247	171	2239/248	178	1301/249
151	0614/247	159	2338/247	172	0040/249	179	1543/249

Downloaded from rsta.royalsocietypublishing.org

if the water were frozen in its position at 0000/248 (hour (G.M.T.)/day number; all dates are given as day of year).

Calibration of the N.B.I.S. CTD data was considerably complicated by two factors. A fast-response thermistor was used to 'speed up' the slower response of the platinum resistance thermometer, by using circuitry within the CTD (Brown 1974). In practice the matching of time constants by this technique is unsatisfactory, and temperature overshoots occur when the temperature gradient changes suddenly, reducing only with the platinum thermometer time constant (about 0.185 s). An *ad hoc* correction algorithm was applied to reduce such overshoots and the induced salinity errors. Remaining salinity errors, estimated by comparison of adjacent up and down traces, are generally less than 0.02‰.

An even more serious error was induced by gradual fouling of the conductivity cell. During long continuous tows in the biologically active surface layer, the 3 cm long, 4 mm wide cell fouls gradually causing derived salinities to be reduced in stages by up to 0.2‰ or more in five to ten hours (Pollard 1980*c*). Fouling events occur several or many times per hour. Fouling is sudden, and often clears completely within a minute or two. But permanent offsets of 0.01 to 0.05‰ occur perhaps once per hour, and these are additive. Calibration during towing is difficult, and was not attempted in JASIN. Luckily, the repeated towing patterns allowed salinity features to be identified in successive circuits, and a set of additive corrections built up, which led to consistent temperature/salinity (T/S) relations over a number of circuits. Absolute calibration was achieved by comparison with T/S curves obtained by other ships in the vicinity (Minnett *et al.* this symposium). After correction, it is estimated that absolute salinity errors are generally less than 0.02‰, and relative salinities less than 0.01‰, with the exception of short periods if the correction was applied at a time different from the time of fouling.

Surface stress and heat fluxes

R.R.S. *Discovery* carries instrumentation to sample meteorological parameters. Sampling is once per second, but data are reduced to two-minute averages before storage. Calibration of all JASIN surface meteorological data is described by Guymer *et al.* (this symposium). For our purposes, surface stress was computed (figure 4*a*) by using the formula of Large & Pond (1982) with wind data only from periods when R.R.S. *Discovery* was head to wind.

The components of surface heat flux (figure 4*b*) were calculated or estimated as follows. Downward shortwave radiation was measured by solarimeter, and ranged from 0 to 500 W m^{-2}. Upward shortwave radiation was estimated, by comparison with net radiometer measurements on R.V. *Meteor*, as 4% of the downward shortwave radiation (error up to 10 W m^{-2}). Net upward longwave radiation was assumed to be constant at 40 W m^{-2} (maximum error, by comparison with R.V. *Meteor*, 30 W m^{-2}). Sensible and latent heat fluxes were calculated from the two-minute averaged data.

On day 247 (4 September 1978) the wind increased from near zero to 15 m s^{-1} (figure 4*a*), and the surface thermocline, which had formed during the preceding calm, sunny days, was eroded to a depth of about 30 m. The temperature at 14 m increased by 0.2 K (figure 2*c*) after noon on day 247 as warm water was mixed down. It then decreased by 0.45 K, mostly owing to entrainment of colder water from below, though advection and surface heat losses (figure 4*b*) account for about 0.15 K of the cooling.

The predominantly westward wind (figure 4*a*) caused northward flow in the surface layer relative to the thermocline, which arrested the southward drift of the spar at about 1800/247

Downloaded from rsta.royalsocietypublishing.org

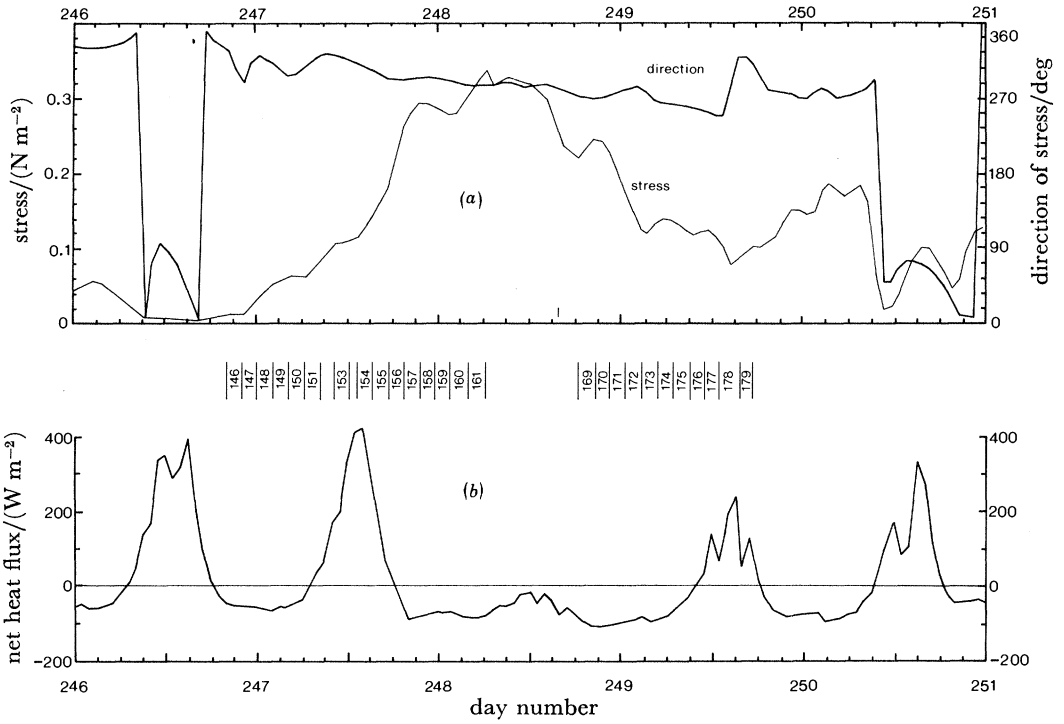

FIGURE 4. Hourly averages of (*a*) surface stress and (*b*) downward heat flux at the sea surface, from two-minute flux averages on board R.R.S. *Discovery*. Wind velocity and wet and dry bulb temperatures have been corrected for ship's heading relative to wind, and fluxes calculated after Large & Pond (1982). The direction given is that towards which the wind is blowing, mostly about 270°, implying an easterly wind. The times of circuits 146 to 179 are also shown.

(figure 1*b*). Windage on the spar thereafter can be estimated from the westward progression of the relative ship track plot (figure 3*b*) at about 10 cm s^{-1}. As the spar drifted westward, the mean current at 42 m decreased (figure 1*b*), implying horizontal shears of order 10^{-5} s^{-1} (1 cm s^{-1} km^{-1}) if the variations were spatial rather than temporal.

3. Mean momentum balance

The object of this paper is to examine changes that occur in the momentum balance when the mixed layer develops in response to a wind event. If horizontal pressure gradients vary little across the surface boundary layer as often assumed (see for example Davis *et al.* 1981; Weller & Halpern this symposium), then any geostrophically balanced currents would be eliminated by examining shears relative to the deepest current meter under the spar (42 m), which was at all times at least 10 m below the base of the mixing layer. Averaged over inertial and tidal periods, the momentum in the surface layer relative to 42 m should then be in Ekman balance, the coriolis force balancing the wind stress. To test this balance, averaged velocity profiles are shown in figure 5.

Before considering the balance of terms, a note on instrumental errors is necessary. Errors in current meter response are evident in the profiles, but we have been unable to determine which current meters are 'right' and which 'wrong', so none has been omitted. The 16 and 25 m VAECMs may be in error owing to sticky compasses, and the 25 m values do look anomalous

PHILOSOPHICAL TRANSACTIONS OF THE ROYAL SOCIETY A MATHEMATICAL, PHYSICAL & ENGINEERING SCIENCES

PHILOSOPHICAL TRANSACTIONS OF THE ROYAL SOCIETY A MATHEMATICAL, PHYSICAL & ENGINEERING SCIENCES

Downloaded from rsta.royalsocietypublishing.org

compared with neighbouring VACMs by 2–3 cm s^{-1}. But if slab-like flow is probable down to 30 m at 0730/248 and 2130/248, then it is the east component of the 14 m VACM that seems anomalously large by about 3 cm s^{-1} by comparison with the 16 m VAECM and 21 and 29 m VACMs. However, in the north component at least, errors of 3 cm s^{-1} are reasonably small compared with the 5–15 cm s^{-1} northward flows in the mixing layer relative to 42 m.

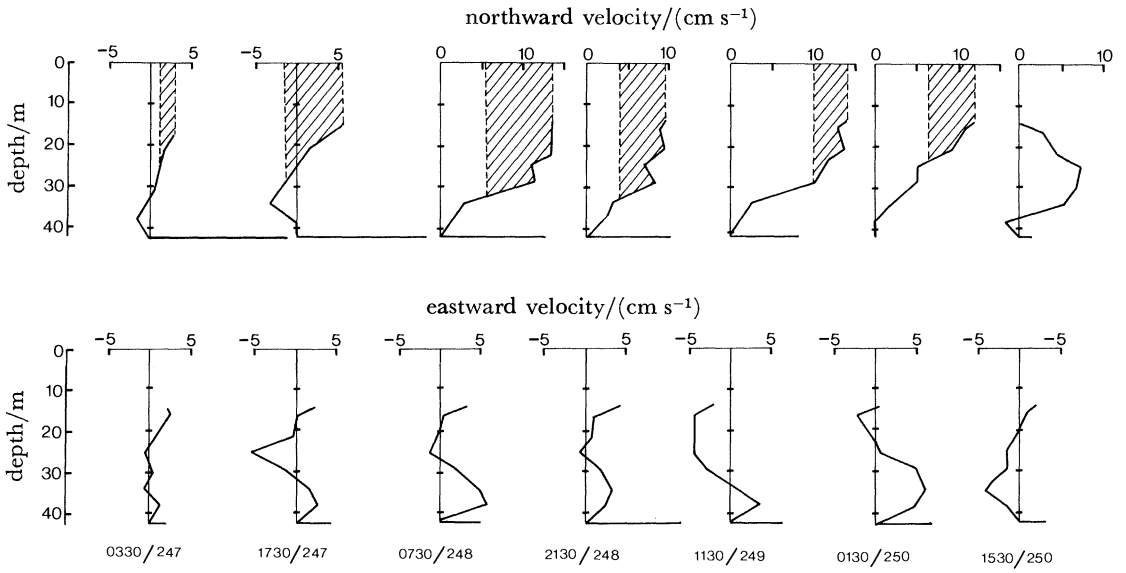

FIGURE 5. Profiles of eastward and northward velocities relative to 42 m under the drifting spar. The values are averaged over fourteen hours centred on the times shown. Absolute southward and westward velocities at 42 m (compare figure 1*b*) are also shown. The momentum that can be accounted for by the Ekman flux during the period the wind blows to the west is hatched on the northward profiles.

The relative northward flow is consistent in direction with the Ekman flux caused by the predominantly westward wind (figure 4*a*), but its magnitude $\tau_x \rho^{-1} f^{-1}$ (shaded in figure 5) is too small, accounting for no more than 60 % of the momentum relative to 42 m at 0730/248 and thereafter. There remains a shear of 4–10 cm s^{-1} between about 30 and 42 m, which cannot be ascribed to instrumental errors, and which is shown by both VACMs (14, 21 and 29 m to 34 and 42 m) and VAECMs (16 and 25 m to 38 m).

Since a simple Ekman balance is not found, estimates of terms in the momentum equations relative to 42 m have been made:

$$\left.\begin{array}{llll} \dfrac{\partial(u-u_{42})}{\partial t} - f(v-v_{42}) + \dfrac{1}{\rho}\dfrac{\partial(p-p_{42})}{\partial x} + \underbrace{\boldsymbol{u}\cdot\nabla u - \boldsymbol{u}_{42}\cdot\nabla u_{42}}_{(10^{-6})} = \dfrac{1}{\rho}\dfrac{\partial \tau_x}{\partial z}, & & & \\ (10^{-6}) \quad (-15\times 10^{-6}) & & & (-10\times 10^{-6}) \\ \dfrac{\partial(v-v_{42})}{\partial t} + f(u-u_{42}) + \dfrac{1}{\rho}\dfrac{\partial(p-p_{42})}{\partial y} + \underbrace{\boldsymbol{u}\cdot\nabla v - \boldsymbol{u}_{42}\cdot\nabla v_{42}}_{(10^{-6})} = \dfrac{1}{\rho}\dfrac{\partial \tau_y}{\partial z}. & & & \\ (10^{-6}) \quad (6\times 10^{-6}) & & & (3\times 10^{-6}) \\ \text{A} \quad \text{B} & & \text{C} & \text{D} \end{array}\right\} \quad (1)$$

The estimates, expressed in m s^{-2}, are derived as follows. (A) Acceleration terms are estimated by comparison of profiles 14 h apart (figure 5). Typical changes in velocity difference between, say,

Downloaded from rsta.royalsocietypublishing.org

29 m and 42 m are 5 cm s^{-1}. (B) For coriolis terms we take $f = 1.25 \times 10^{-4}$ s^{-1}, $v - v_{42} = 12$ cm s^{-1}, $u - u_{42} = 5$ cm s^{-1}. (C) Stress terms are estimated by assuming that surface stress ($\tau_x = -0.3$ N m^{-2}, $\tau_y = 0.1$ N m^{-2}) reduces to zero linearly over 30 m. (D) Invoking Taylor's hypothesis applied to the 42 m absolute velocities plotted on figure 1*b*, one can estimate $\partial u_{42}/\partial x$ and $\partial v_{42}/\partial x$ as 10^{-5} s^{-1}. If $\partial \boldsymbol{u}/\partial x$ is independent of z, and $\boldsymbol{u} - \boldsymbol{u}_{42}$ is about 10 cm s^{-1}, then D is $O(10^{-6}$ m s$^{-2})$.

The acceleration and nonlinear terms are an order of magnitude smaller than the coriolis and stress terms, and tend to cancel each other ($\mathrm{D}\boldsymbol{u}/\mathrm{D}t = 0$) as temporal changes are induced by the translation of the spar through the water. But we have shown that the coriolis and stress terms do not balance. Hence the balance must be completed by the pressure gradient difference term, and the original hypothesis that pressure gradients vary little across the boundary layer is incorrect. Rather, that part of the coriolis term not balanced by the stress must be in geostrophic balance with the pressure gradient term. How do the pressure gradients arise?

Geostrophic balance

To examine the geostrophic balance we need to examine the density field, from which vertical pressure differences ($p - p_{42}$) can be derived by using the hydrostatic equation. Examination of figure 5 shows that the non-wind-driven velocity shear lies between 30 and 40 m, and is of order 10^{-2} s^{-1}. To balance such shear requires a pressure gradient difference term of order 5×10^{-6} m s^{-2}, from equations (1). The hydrostatic equation then yields

$$-\frac{g}{\rho}\int_{-40}^{-30}\frac{\partial \rho(x,z)}{\partial x}\,\mathrm{d}z = \frac{1}{\rho}\left(\frac{\partial p_{30}}{\partial x} - \frac{\partial p_{40}}{\partial x}\right) = 5 \times 10^{-6}\ \mathrm{m\,s^{-2}}$$

so that the depth-averaged value of $\partial\rho/\partial x$ between 30 and 40 m must be 0.05 kg m^{-3} km^{-1}. Finally, we can estimate the slope $\partial H/\partial x$ of an isopycnal surface using the relation

$$\frac{\partial H}{\partial x} = \frac{-\partial\rho/\partial z}{\partial\rho/\partial x} \tag{2}$$

given estimates of $\partial\rho/\partial z$. From figure 6, $\partial\rho/\partial z$ varies from 0.002 kg m^{-4} or less in the surface layer (profiles 156–158), through 0.02 kg m^{-4} mean thermocline gradient (e.g. profile 159) to a maximum of 0.2 kg m^{-4} immediately below the base of the mixing layer (e.g. profile 169). These estimates yield, respectively, $\partial H/\partial x = 25$, 2.5 and 0.25 m km^{-1}. Ruling out the first value, we seek a slope in isopycnal surfaces or in the mixed-layer depth (MLD) of order 10^{-3}, or 1 m km^{-1}.

Three estimates of MLD are plotted in figure 7*a*. Two are derived from the depths of the density surface $\sigma_T = 26.7$ kg m^{-3} from side-averaged profiles, some of which are shown in figure 6. Between circuits 159 and 161 (0000 to 0600/248) the MLD increased from under 20 m to 40 m. Thereafter, despite the poor spatial averaging (figure 6, caption), the MLD is persistently shallower by about 5 m on the south-side averaged profiles than on the north side. The third estimate of MLD is derived from the VACM temperature records (figure 2*c*) under the spar, which show that the MLD oscillated with a range of 10–15 m both before and after the onset of mixing. For example, the temperature at all depths down to 34 m increases by up to 0.2 K between 0900/247 and 1700/247 owing to vertical advection by the ten-hour period internal wave apparent in figure 2*c*. Thus the MLD is over 30 m at 1700/24, but reduces again to less than 14 m by 2000/247.

Isotherm depths were deduced by linear interpolation between the temperature sensors, and the depth of an isotherm marginally colder than the mixed-layer temperature (MLT) is an estimate of MLD (t). As the MLT decreases, the isotherm must be changed, yielding the composite

PHILOSOPHICAL TRANSACTIONS OF THE ROYAL SOCIETY A MATHEMATICAL, PHYSICAL & ENGINEERING SCIENCES
PHILOSOPHICAL TRANSACTIONS OF THE ROYAL SOCIETY A MATHEMATICAL, PHYSICAL & ENGINEERING SCIENCES

Downloaded from rsta.royalsocietypublishing.org

estimate of MLD beneath the drifting spar (figure 7*a*, dashed line). We now have three estimates of MLD, which are significantly different by day 249. MLD is shallowest at the drifting spar, about 25 m. It deepens to the east of the spar, as the south-side average is 30 m, and it deepens further to the north, the north-side average being 35 m. Thus the MLD slopes downwards by about 1 m km^{-1} towards the east and north, which is the magnitude required by the foregoing calculation. The slope persists for more than a tidal period, which rules out internal waves as the cause.

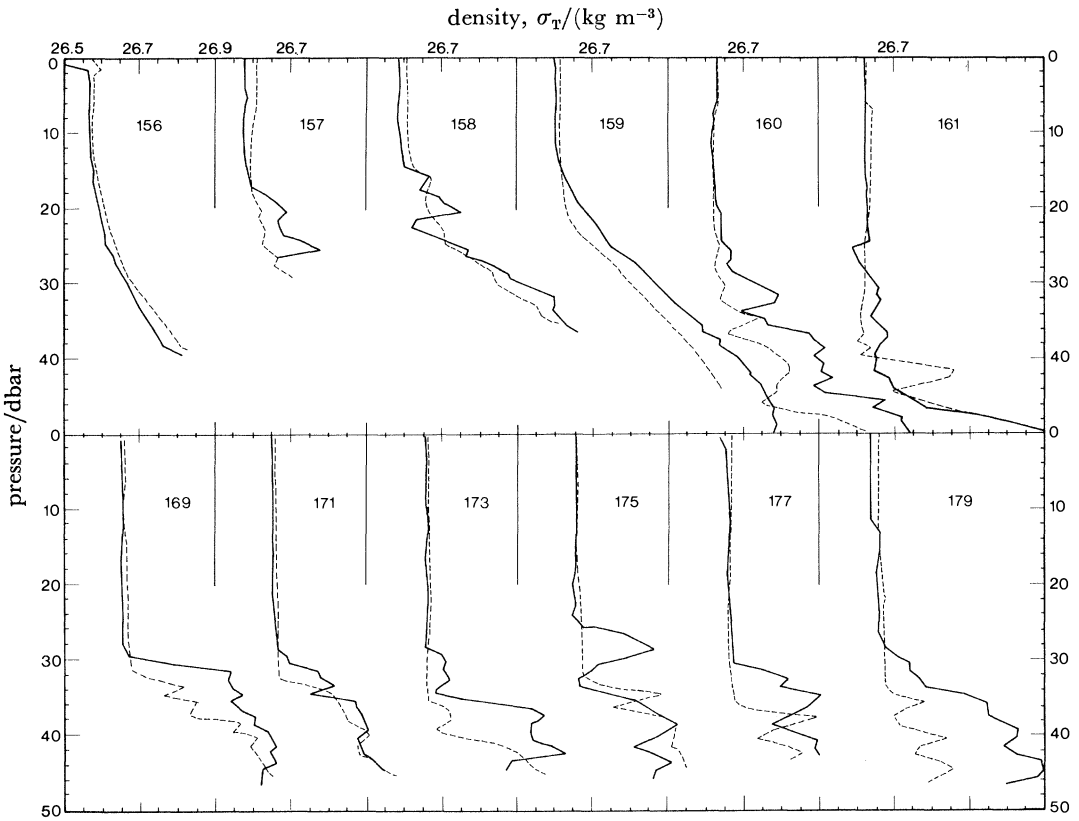

FIGURE 6. Density profiles averaged on pressure along the southern (solid) and northern (dashed) sides of each circuit. Each side generally contains two or three 'fast' (slope of 1 in 5 to the horizontal) down traces and one or two 'slow' (1 in 100) up traces. Apparent density inversions are artefacts, caused by inadequate averaging of horizontal variations. Circuits 156 and 159 are exceptions, consisting of fast down and up traces (25 and 11 down-and-ups per side respectively), which yield the smoother monotonic profiles. Times of circuits are given in table 1.

Is the slope in the correct sense? The downward slope to the east requires a northward velocity in the mixed layer relative to 42 m for geostrophic balance, in agreement with figure 5. The downward slope to the north requires westward velocity in the mixed layer relative to the thermocline, and such shear is generally present between 29 m and 38 m in the east profiles of figure 5. But the eastward Ekman flow due to the north component of the wind stress, coupled with instrumental errors and the unexplained shear reversal between 38 and 42 m, renders the comparison less convincing than that for the northward component of velocity.

There is one occasion on which detailed geostrophic shear profiles can be estimated from the density profiles. During circuit 178 (1300/249) 25 density profiles were obtained along the 7 km south side. Individual profiles (not shown) showed the depth of the 26.7 kg m^{-3} density contour

Downloaded from rsta.royalsocietypublishing.org

increasing by about 10 m in 5 km starting from the drifting spar position. Figure 7*b* shows two averaged density profiles from (i) the first seven profiles spanning 2.0 km (solid line), and (ii) the next nine profiles spanning the next 2.7 km (dashed line). The profiles were averaged first by calculating the average density in 1 dbar intervals of pressure, and second by calculating the average pressure in 0.02 kg m^{-3} intervals of density. Averaging density on pressure is necessary where the density gradient is weak (the mixed layer), but smears out the vertical gradients of density near the base of the mixing layer. Averaging pressure on density surfaces retains these sharp density gradients. The profiles derived by the two procedures were overlaid and the smoothed profiles of figure 7*b* traced off.

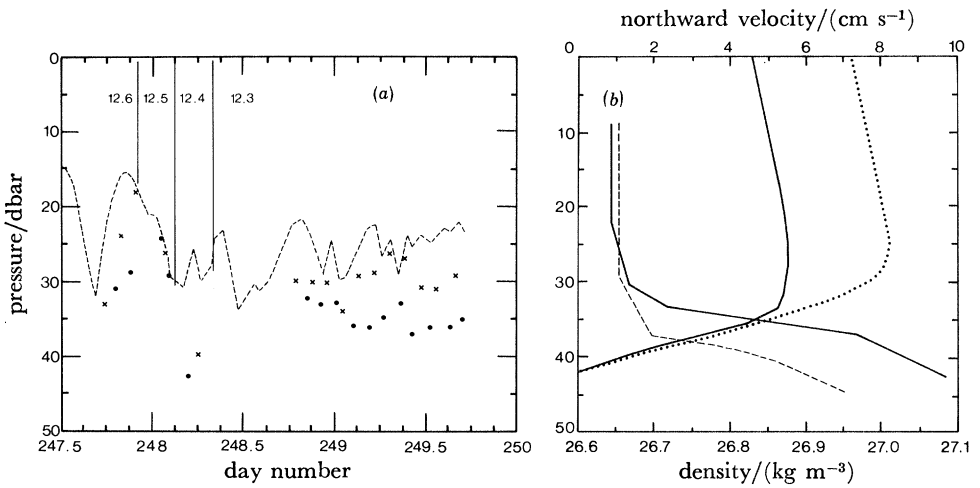

FIGURE 7. (*a*) MLDs estimated from (i) isotherm depths under the drifting spar (dashed line) for isotherms 12.6 to 12.3 °C as shown, and (ii) the depths of the density surface $\sigma_T = 26.7$ from averaged profiles (figure 6) along the south (crosses) and north (dots) sides of circuits 154 to 179. (*b*) Density profiles from the south side of circuit 178 averaged over seven (solid line) and nine (dashed line) individual profiles. The solid profile was centred 2.35 km west of the dashed, yielding the northward geostrophic velocity profile (solid line) shown relative to 42 m. Similarly, the dotted line is the geostrophic velocity profile 2 h later, from averaged density profiles 4.4 km apart during circuit 179.

Since the data were collected over a 20 min period, there is no way of eliminating internal waves with horizontal scales greater than 2 km, in particular the tide. However, the 26.7 kg m^{-3} density surfaces are 4.5 dbar apart on the averaged profiles, consistent with the 5 dbar difference between MLDs under the spar and 7 km south-side averages (figure 7*a*), which persisted for more than an inertial period prior to run 178. We argue therefore that the two profiles are representative of conditions that persisted long enough for geostrophic balance to be established, and the geostrophic velocity profile above a reference level of 42 m, given the 2.35 km mean separation of the density profiles, is also shown (solid line) in figure 7*b*.

There is a 5 cm s^{-1} shear between 34 and 42 dbar, similar in amplitude to and in the correct direction to account for the non-wind-driven shears on figure 6 (1130/249 north profile). The calculation was repeated for circuit 179, and the geostrophic velocity profile, in this case from averaged density profiles 4.4 km apart, is shown (dotted line) in figure 7*b*. The shear from 28 to 42 dbar is 8 cm s^{-1}. Figure 7*b* confirms that it is the slope of the MLD that accounts for most of the shear of order 10^{-2} s^{-1} across the seasonal thermocline.

Downloaded from rsta.royalsocietypublishing.org

Geostrophic adjustment

It remains to examine the role of wind mixing in generating the variations in MLD. Two temperature profiles (figure 8*a*, I) were chosen representing the range of profiles observed around 1400/247, before the main wind event. The profiles were then modified by incorporation of a mixed layer with temperature appropriate to that at the end of the wind event (2100/248). The MLD was determined by conservation of heat, mixed-layer cooling being dominated by entrainment of cold water from the thermocline. Heat loss through the surface (figure 4*b*) was allowed for, but affected the final MLDs (F) by less than 1 m. If the four profiles are converted to density profiles (ignoring salinity), and taken to be 7 km apart (i.e. on the north and south sides of the ship circuits), one can as before calculate the 'initial' and 'final' geostrophic velocity profiles relative to 40 dbar (figure 8*b*).

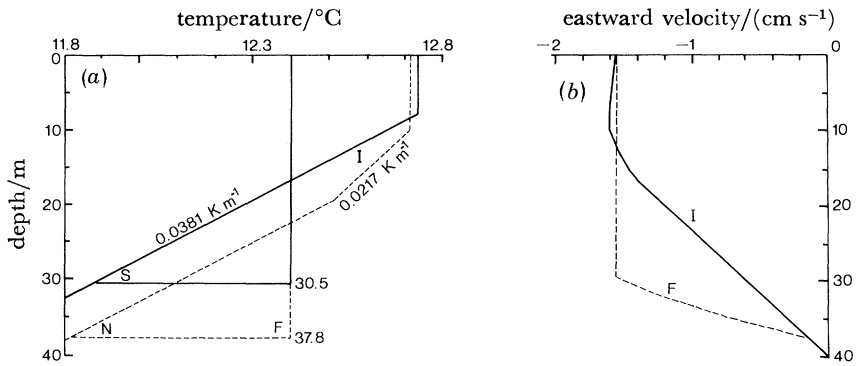

FIGURE 8. (*a*) Two examples (S and N) demonstrate the differences in MLD that are inferred from two initial profiles when the surface heat flux and the cooling rate of the mixing layer are known. Initial temperature profiles I are approximations to observed profiles during circuit 154 (1400/247). Final profiles F would then occur during circuit 170 (2100/248). (*b*) Initial (I) and final (F) eastward geostrophic velocity profiles relative to 40 dbar, estimated from the modelled temperature profiles in figure 8*a*, assuming the solid profiles were 7 km south of the dashed profiles.

Wind mixing rearranges the vertical density gradients. If horizontal density gradients (and hence geostrophic shear) existed prior to the storm, then the mixing process is likely to result in a deeper MLD at one place than another (figure 8*a*). In other words the horizontal density gradients are also rearranged by the mixing in such a way that the shear becomes concentrated across the base of the mixing layer. Note that the mass of water between the surface and a point deeper than the level to which the mixing penetrates is unchanged in the absence of surface heat fluxes. Hence the total velocity difference between those two points is also unchanged, as shown in figure 8*b* between 0 and 40 dbar.

While figure 8*b* demonstrates that wind-driven turbulence in the surface layer has the potential to modify pressure gradients, that appears for two reasons not to be the primary cause of the observed shears (figure 5). First, there are temporal changes in the non-Ekman northward velocity differences $v - v_{42}$ between the slab-like mixing layer and 42 m (-2 cm s^{-1} at 1730/247, 5 cm s^{-1} at 0730/248, 10 cm s^{-1} at 1130/249). Second, large changes in the velocity shear occur when there is no strong wind driving (e.g. around 1130/249). Further study is required, but the temporal variations may reflect either horizontal variations in vertical shear observed as the spar drifts past them, or temporal variations in the geostrophic balance as confluence $\partial u/\partial x$ compresses horizontal density and pressure gradients (MacVean & Woods 1980).

PHILOSOPHICAL TRANSACTIONS OF THE ROYAL SOCIETY A MATHEMATICAL, PHYSICAL & ENGINEERING SCIENCES
PHILOSOPHICAL TRANSACTIONS OF THE ROYAL SOCIETY A MATHEMATICAL, PHYSICAL & ENGINEERING SCIENCES

Downloaded from rsta.royalsocietypublishing.org

4. Inertial oscillations

Turn now to the inertial period response. While tides dominate the absolute velocities (figure 2), it can be shown that they are largely eliminated by considering shears, as follows. Consider a tide (or other internal wave) for which the surface boundary condition $w = 0$ forces vertical dependence of the form

$$F(x, y, z, t) = F_1(x, y, t) \cos kz \quad (F_1 = u, v \text{ or } p)$$
$$w(x, y, z, t) = w_1(x, y, t) \sin kz.$$

As long as 42 m is deeper than the first node of $\cos kz$, i.e. $2\pi/k > 42$ m, we can approximate the z-dependence by $F = F_1$, $w = kzw_1$. It follows that such a wave can only contribute to equations (1) through nonlinear terms such as $(u - u_{42})\,\partial u/\partial x$ where the horizontal shear may be tidal but the vertical velocity difference is non-tidal.

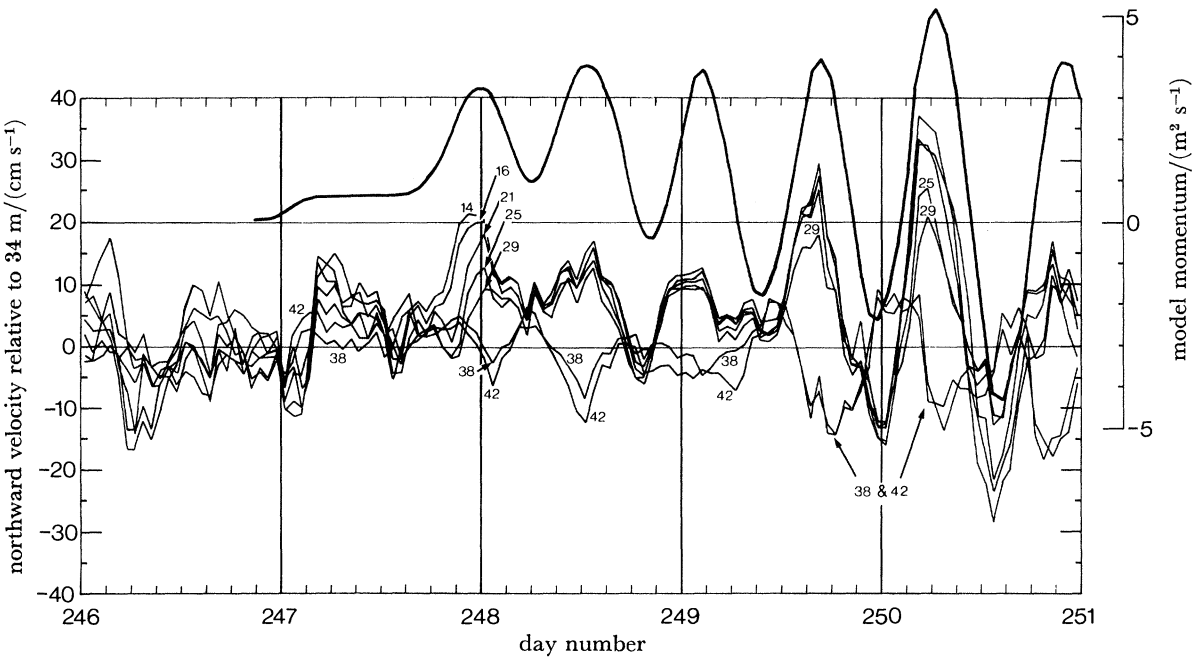

Figure 9. North component of velocity relative to 34 m for current meters at 14, 16, 21, 25, 29, 38 and 42 m. The upper curve is the north component of the momentum response to the Pollard & Millard (1970) model driven by the wind stress of figure 4*a*.

The time series of hourly-averaged velocities relative to a 34 m reference level is shown in figure 9. For brevity, only the northward component is shown. Shears are confused until 1800/247 when the increasing wind stress sets in motion oscillations at 14, 16, 21, 25 and 29 m in succession (around 0000/248) as the mixing layer deepens to 30 m. Thereafter the motion is independent of depth (slab-like) down to 29 m within the instrumental differences of a few centimetres per second until 1200/249. The stress has by then decreased from 0.3 N m^{-2} to 0.1 N m^{-2} (figure 4*a*), and first the 29 m velocity (1500/249) and later the 25 m velocity (0500/250) become distinguishable from the shallowing slab-like behaviour.

Downloaded from rsta.royalsocietypublishing.org

The smooth upper curve on figure 9 is the modelled north (V) component of momentum in response to the vertically integrated Pollard & Millard (1970) model

$$\frac{\partial U}{\partial t} - fV = \frac{\tau_x}{\rho}, \quad \frac{\partial V}{\partial t} + fU = \frac{\tau_y}{\rho} \tag{3}$$

initialized with zero velocities at 2000/246, when the wind stress was negligible. For the short-period (three days) response considered here even the damping/dispersion term used by Pollard & Millard has been omitted. It can be seen that the phases of the observed velocities relative to 34 m are in reasonable agreement with the modelled response, verifying that the observed response is at near-inertial frequency and that tides appear to have been largely eliminated. To quantify that statement, we have carried out complex demodulation at the inertial period (14 h), on 14 h pieces of the time series (figure 10) overlapped by 7 h. The phases (figure 10*c*) of the observations (relative to a pure inertial oscillation) are constant within 30° throughout days 248 and 249, which is a reassurance that the amplitudes are not contaminated by tidal or other periodic shear, in spite of the short piece lengths.

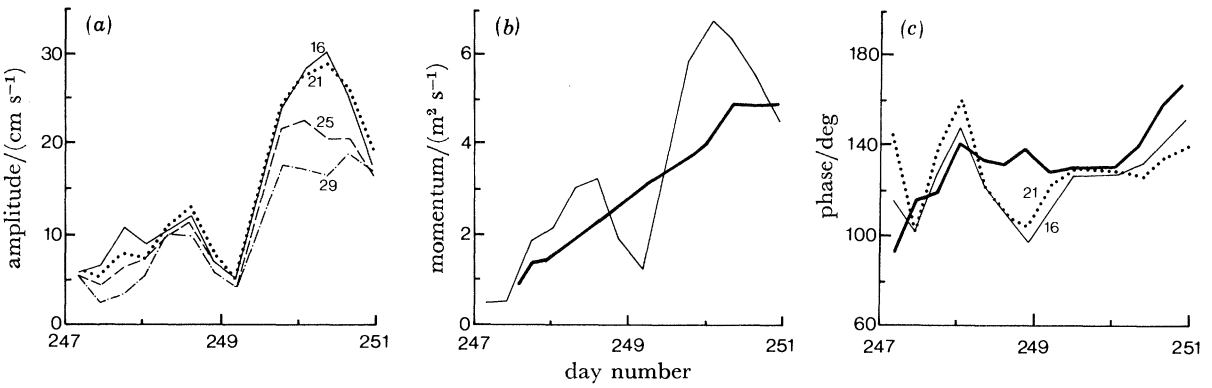

FIGURE 10. Complex demodulation at inertial frequency of shears relative to 42 m. (*a*) Inertial amplitude at 16 m (solid line), 21 m (dotted line), 25 m (dashed line) and 29 m (dash–dot line); (*b*) observed inertial momentum (thin line) estimated by integrating the amplitudes (*a*) down to the observed MLD (figure 7*a*), and modelled momentum (bold line) from the Pollard & Millard (1970) model (compare figure 9); (*c*) phase of inertial oscillations at 16 m (thin line) and 21 m (dotted line) and of modelled response (bold line).

The amplitudes of the inertial oscillations at a selection of levels are shown in figure 10*a*, and in figure 10*b* those amplitudes have been vertically integrated down to the 14 h mean observed MLD, taken from the isotherm depths (dashed line, figure 7*a*), and plotted as integrated inertial momentum (thin line) for comparison with the modelled inertial momentum (bold line), obtained by complex demodulation of the model response. While observed and modelled momentum both trend upwards from 0 to 5 $m^2 s^{-1}$ over 4 days, there are striking differences far in excess of possible instrumental errors. Around 1200/248 and 0000/250 observed values are 50 % greater than modelled, amounting to up to 10 $cm s^{-1}$ distributed through 30 m. Early on 249, on the other hand, observed amplitudes are less than 50 % of modelled values.

The explanation of the discrepancies is not obvious. The model (equation (3)) omits only pressure gradient and nonlinear terms. Pressure gradient terms corresponding to near-inertial but not exactly inertial frequencies are responsible for gradual dispersion of near-inertial momentum out of the mixing layer, and were modelled as a decay term by Pollard & Millard (1970). But inclusion of such terms would reduce modelled amplitudes, the opposite of the 50 % increase we seek.

Downloaded from rsta.royalsocietypublishing.org

Advective changes can be ruled out because the spar drift relative to the slab motion of the mixing layer was only 10 km day^{-1}, but the near-inertial motion observed must have a horizontal scale of at least tens of kilometres (Pollard 1980*a*).

Inertial oscillations are most effectively generated by sudden changes in forcing with a time scale of a few hours, or f^{-1} (Pollard & Millard 1970), but there is no change in wind stress large enough to account for the rapid onset of oscillations on day 249.

We can see two possible explanations. (i) In the process of geostrophic adjustment, horizontal pressure gradients may change rapidly enough to generate inertial oscillations. (ii) The strong tidal oscillations may exchange momentum with the inertial oscillations.

To allow comparison between these alternatives, we began by calculating the functions $F(z) = \partial(u_z - u_{42})/\partial t - f(v_z - v_{42})$ and $G(z) = \partial(v_z - v_{42})/\partial t + f(u_z - u_{42})$ from the current records. To reduce high frequency internal wave noise, one-hour averages were calculated and then

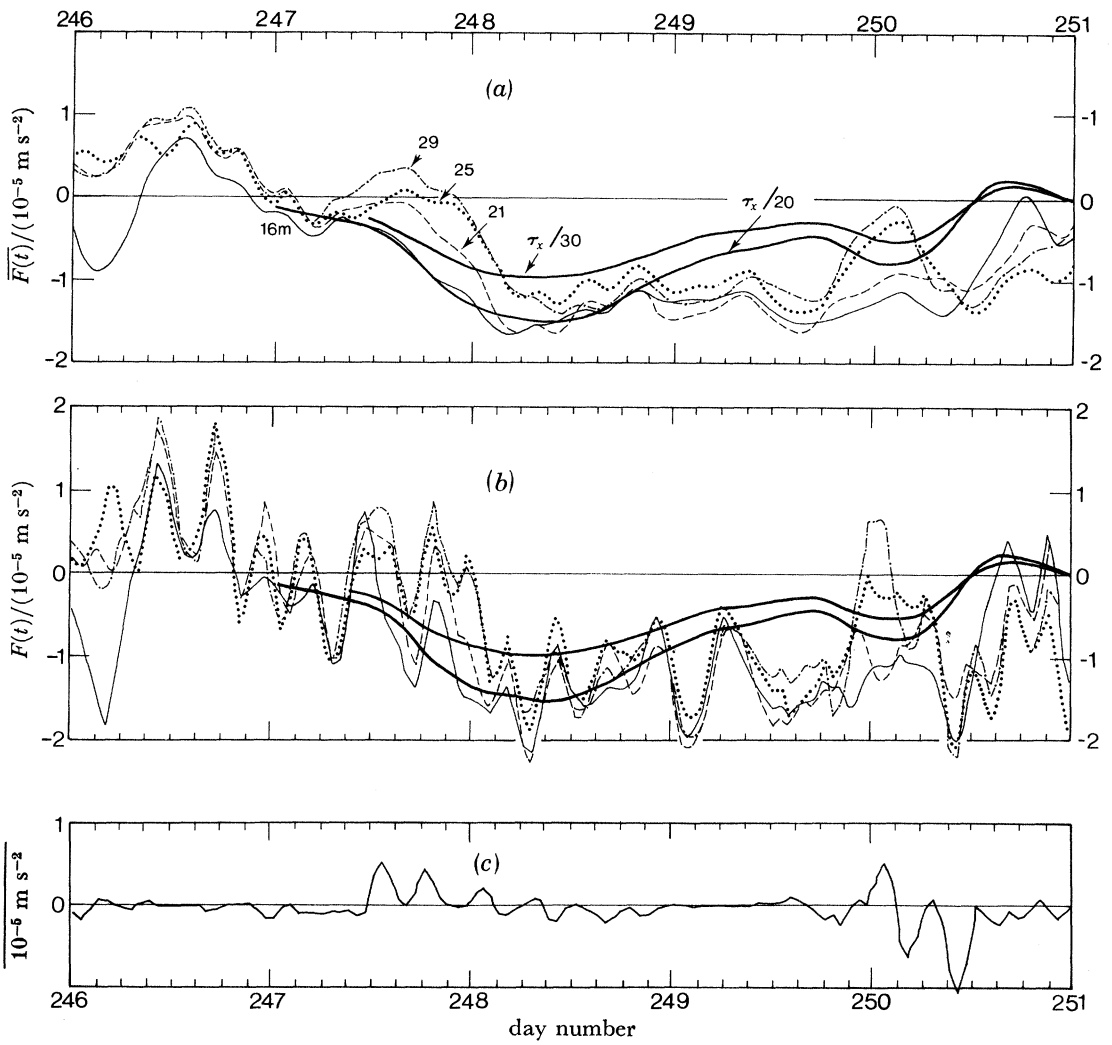

FIGURE 11. The function $F(t) = \partial u/\partial t - fv$ for current records at 16 m (thin lines), 21 m (dashed lines), 25 m (dotted lines) and 29 m (dash–dot lines) relative to 42 m is shown (*a*) after averaging with a nine-hour running mean (*b*) without averaging. Two estimates of $d\tau_x/\partial z$, are also shown (bold lines). The function $(u_{16} - u_{42})\partial w/\partial z$ is shown in (*c*) as an example of tidal–inertial interaction. If there were no *y*-derivatives, it would be the same as $-(u_{16} - u_{42})\partial u/\partial x$.

Downloaded from rsta.royalsocietypublishing.org

further smoothed by taking a three-hour running mean. Function F is shown in figure 11*b*. It shows a marked 6–9 h periodicity, and so was further smoothed with a nine-hour running mean (figure 11*a*). Superimposed on both plots are the functions τ_x/H with $H = 20$ m and 30 m, indicative of the range of $\partial\tau_x/\partial z$. Linear decay of the stress through the mixing layer is a good approximation in view of its slab-like behaviour.

Tidal interactions

To investigate the role of tides, we need an estimate of their horizontal wavelength. An estimate can be obtained in two ways. (i) Suppose the 10 h periodicity (figure 2*c*) is caused by a 12.4 h tide Doppler-shifted by the 15 cm s^{-1} mean southward velocity. That would require a 28 km wavelength in the y-direction. (ii) From a time series of isotherm depths, the amplitude A of the 10 h oscillations was estimated and compared with the mean depth z of the isotherm. For both the 11.5 and 12.0 °C isotherms, the calculation yielded $A = 0.23\,z$. So let the internal wave amplitude be given by $\eta = A \sin \omega t$ with $\omega = 2\pi/10\,\mathrm{h}^{-1}$. Then $w = A\,\omega \cos \omega t$, and

$$\partial w/\partial z = 0.23\,\omega \cos \omega t = 4 \times 10^{-5} \cos \omega t \ \mathrm{s}^{-1}. \tag{4}$$

If the tide is a plane wave propagating in the horizontal direction r, then by continuity $\partial u_r/\partial r = -\partial w/\partial z$. Taking 15 cm s^{-1} as the amplitude of u_r yields 24 km for the horizontal wavelength.

The two estimates are independent, one based on the period, the other on the amplitude of the tidal internal wave. The short 25–30 km estimated wavelength (cf. Levine *et al.* this symposium) results in large horizontal velocity gradients of up to 4 cm s^{-1} km^{-1} (from (4)), which contribute to the nonlinear terms in (1) through terms like $(u_\mathrm{I} - u_{\mathrm{I},\,42})\,\partial u_\mathrm{T}/\partial x$, as shown earlier (subscripted I for inertial, T for tidal). Inserting typical values of the inertial shear from figure 10 yields $(0.1 - 0.3) \times 4 \times 10^{-5}\,\mathrm{m\,s^{-2}} = (0.4 - 1.2) \times 10^{-5}\,\mathrm{m\,s^{-2}}$ for the amplitude of tidal–inertial interactions. The periodicities of the interaction term, from the sum and difference frequencies of the 14 h inertial oscillation and 10 h tide, would be 6 and 35 h.

Without knowing the direction of propagation of the tide we cannot calculate the nonlinear terms for detailed comparison with figure 11*b* (although an example is shown in figure 11*c*) but the marked 6 h periodicity with amplitudes consistent with the foregoing estimate is strongly indicative of tidal–inertial interaction. But the rapid (6 h) oscillation of momentum between inertial and tidal motions is on too short a time scale to account for the longer period changes in the inertial amplitude (figure 10*b*), and it may only be coincidental that the two maxima in the inertial amplitude are 35 h apart.

Pressure gradients

Is it possible that rapidly changing pressure gradients modify the inertial oscillations? Examine first the oscillations generated during the initial mixing phase. Until 0000/248, the smoothed values of F (16 m) (figure 11*a*) are balanced by the vertical gradient of τ_x for a MLD of 20 m. Since the observed MLD (figure 7*a*) was 15–20 m between 1800/247 and 0000/248, pressure gradients are not required to complete the momentum balance, i.e. equations (3) hold, after smoothing of tidal–inertial interactions. But between 0000 and 0400/248 the mixed layer deepened rapidly (compare profiles 159 and 161, figure 6), from about 21 m to, say, 28 m after smoothing of tidal variations (figure 7*a*). In the same period F (16 m) changed by $0.5 \times 10^{-5}\,\mathrm{m\,s^{-2}}$ from -1.25×10^{-5} to $-1.75 \times 10^{-5}\,\mathrm{m\,s^{-2}}$, but $\rho^{-1}\partial\tau_x/\partial z$ decreased from $-1.3 \times 10^{-5}\,\mathrm{m\,s^{-2}}$

PHILOSOPHICAL TRANSACTIONS OF THE ROYAL SOCIETY A MATHEMATICAL, PHYSICAL & ENGINEERING SCIENCES
PHILOSOPHICAL TRANSACTIONS OF THE ROYAL SOCIETY A MATHEMATICAL, PHYSICAL & ENGINEERING SCIENCES

Downloaded from rsta.royalsocietypublishing.org

($0.28\,\mathrm{N\,m^{-2}}$ across 21 m) to $-1.1\times10^{-5}\,\mathrm{m\,s^{-2}}$ ($0.31\,\mathrm{N\,m^{-2}}$ across 28 m). If pressure gradient terms complete the momentum balance, then their amplitudes would have to be as follows (in $\mathrm{m\,s^{-2}}$):

$$F(16\,\mathrm{m})-\rho^{-1}\partial\tau_x/\partial z = -\rho^{-1}(\partial p_{16}/\partial x-\partial p_{42}/\partial x),$$

$$\text{before:}\quad -1.25\times10^{-5}+1.3\times10^{-5}=0.05\times10^{-5},$$

$$\text{after:}\quad -1.75\times10^{-5}+1.1\times10^{-5}=-0.65\times10^{-5}.$$

The change in pressure gradient ($0.7\times10^{-5}\,\mathrm{m\,s^{-2}}$) is about half the change in stress ($1.3\times10^{-5}\,\mathrm{m\,s^{-2}}$) due to the earlier increase in wind, and so can potentially contribute significantly to the generation of inertial oscillations, if the pressure gradient changes fast enough. What we cannot prove is that the pressure gradients adjusted, not in the 14 h between 1730/247 and 0703/248, but in the 4 h from 0000 to 0400/248. But if the pressure is hydrostatic it depends on the density field, and certainly the south-side average density profiles adjusted in four hours (159–161, figure 6), so it is reasonable to assume the horizontal density gradients did also.

Put another way, the coriolis force on the mean north velocity shear at 0730/248 can be balanced by apportioning two thirds to the stress and one third to pressure gradients. Similarly, the inertial amplitudes are 50 % larger than can be explained by the rate of change of the wind stress, so the excess may very well be due to the rate of change of the pressure gradients.

The same argument can be applied to the increase in inertial amplitude on day 249. Then the non-Ekman mean shear increased from $5\,\mathrm{cm\,s^{-1}}$ at 2130/248 to $10\,\mathrm{cm\,s^{-1}}$ at 1130/249, which we could only ascribe to confluence or convergence $\partial u/\partial x$ of unknown origin moving columns of water closer together, so enhancing horizontal pressure gradients. If that confluence occurred fast enough it could enhance the inertial oscillations as observed, and we note that the decrease in the smoothed function $F(16\,\mathrm{m})$ (figure 11*b*) took 4 h from 0900 to 1300/249.

In conclusion, both rapid geostrophic adjustment and tidal–inertial interactions could be responsible for the varying amplitudes of figure 10*b*. We believe at present that geostrophic adjustment is the more likely contender because the pressure gradients deduced from mean non-wind-induced shears do change with the right sign and size, although their rate of change cannot be reliably determined in the presence of variations caused by tidal–inertial interactions.

5. Summary and conclusions

The experiment described in this paper was designed to explore the structure of the upper ocean on scales from a few metres to ten kilometres, and from hours to days, and to reveal the physical processes involved in wind-driven mixing. An essential prelude to such detailed examination is to understand the mean heat, momentum and energy budgets. Since the momentum balance alone was more complex than expected, we have chosen to concentrate on it in this paper.

Observations of the development of the mixing layer as the wind speed increased to $15\,\mathrm{m\,s^{-1}}$, and remained high for a day, revealed two problems in achieving a balanced momentum budget. These were (i) mean shears of up to $0.01\,\mathrm{s^{-1}}$ developed just below the base of the mixed layer over and above what could be attributed to the mean wind-driven Ekman flux, and (ii) inertial oscillations of up to $30\,\mathrm{cm\,s^{-1}}$ developed in the mixed layer, larger by up to 50 % than could be generated by using the time-varying wind stress in the Pollard & Millard (1970) model.

In an attempt to explain the observations, the momentum budget has been examined in some detail. Our conclusions are as follows.

PHILOSOPHICAL TRANSACTIONS OF THE ROYAL SOCIETY A MATHEMATICAL, PHYSICAL & ENGINEERING SCIENCES

PHILOSOPHICAL TRANSACTIONS OF THE ROYAL SOCIETY A MATHEMATICAL, PHYSICAL & ENGINEERING SCIENCES

Downloaded from rsta.royalsocietypublishing.org

(*a*) The part of the mean shear not balanced by the wind stress is in geostrophic balance. The shear is concentrated between 30 and 40 m and the horizontal density gradients required to balance it are primarily due to the slope of the MLD. Slopes in MLD of 10^{-3} were found, causing the mixed layer to slope from 25 m to 35 m across a 7 km square.

(*b*) Horizontal density gradients present before a wind event result in a slope in MLD after the wind event. Thus geostrophically balanced shears present before the wind event become concentrated at the base of the mixing layer as the mixing rearranges vertical and hence horizontal density gradients.

(*c*) There is evidence for enhancement of horizontal density gradients and hence of geostrophically balanced shears by confluence or convergence.

(*d*) Tidal–inertial interactions were present (with a beat-period of about 6 h), and had similar amplitudes to the wind stress gradient $\partial\tau/\partial z$. However, the time series was too short to investigate whether the other beat period (35 h) could be the explanation of the varying inertial amplitudes. The possibility cannot be ruled out.

(*e*) We favour the hypothesis that the pressure gradient adjustment described by (*b*) or (*c*) took place fast enough (within a few hours) to account for the variations in inertial amplitude that were observed, when added to the rate of change of the wind stress. The amplitude and signs of the changes in 14 h mean geostrophic velocity shears were consistent with this hypothesis, and there was some evidence to support the rapid adjustment.

Other observations to support our findings on the role of pressure gradients in the near-surface momentum budget are rare, because of the difficulty of obtaining detailed hydrographic data. Gregg (1976) had such data, and reports an example of the mixed layer deepening from 10 to 110 m in 7 km. Weller & Halpern (this symposium), using two-month time series spanning the whole of JASIN 1978, found that the current response that was coherent with the wind was not in Ekman balance, nor did the inertial oscillations obey Pollard & Millard's (1970) model (Weller 1982). Davis *et al.* (1981) lacked hydrographic data, but inferred that accelerations observed during storms were associated with pressure gradients that were strongly depth dependent. They also noted spectral peaks resulting from nonlinear interactions between the tidal and inertial frequency bands.

Although Pollard & Millard's (1970) model has often been found to explain surface wind-generated inertial oscillations, it rarely accounts for all the inertial events in a record (see for example Pollard & Millard 1970; Kundu 1976; Weller 1982). As an alternative to the suggestions discussed in this paper, Weller argued that convergences associated with the observed eddies (Ellett *et al.* this symposium) could modify the amplitudes of inertial oscillations through nonlinear terms.

A dramatic example of MLD variations is given by Andrews & Scully-Power (1976), in which the mixed layer deepens from 100 to 300 m from edge to centre of an intense eddy of radius less than 100 km. While that may be an exceptional example, it seems plausible to conclude that MLD variations and the geostrophically balanced shears that accompany them are likely to occur wherever there are fronts or eddies in the ocean.

Among the many people who made this experiment such a success were the Master and crew of R.R.S. *Discovery*, whose navigational excellence is clear in the track plots, I. Waddington (drifting spar), C. Clayson (VAECMS), P. Gwilliam (SST), J. Smithers (CTD), V. Lawford (Sea-Soar), and members of the shipborne computer group, especially B. Lewis and J. Burnham

PHILOSOPHICAL TRANSACTIONS OF THE ROYAL SOCIETY A MATHEMATICAL, PHYSICAL & ENGINEERING SCIENCES

PHILOSOPHICAL TRANSACTIONS OF THE ROYAL SOCIETY A MATHEMATICAL, PHYSICAL & ENGINEERING SCIENCES

Downloaded from rsta.royalsocietypublishing.org

(Sea-Soar computer). Initial data reduction was done by D. Collins and Mrs M. White. Especial thanks are due to Margaret White, who helped immeasurably as personal assistant to me and to the JASIN project.

References

Andrews, J. C. & Scully-Power, P. 1976 The structure of an East Australian Current anticyclonic eddy. *J. phys. Oceanogr.* **6**, 756–765.

Brown, N. L. 1974 A precision CTD microprofiler. *IEEE International Conference on engineering in the ocean environment record, Ocean* '74, vol. 2, pp. 270–278.

Davis, R. E., De Szoeke, R., Halpern, D. & Niiler, P. 1981 Variability in the upper ocean during MILE. Part 1. The heat and momentum balances. *Deep-Sea Res.* **28**A, 1427–1451.

Dessureault, J. G. 1976 'Batfish'. A depth controllable towed body for collecting oceanographic data. *Ocean Engng*, **3**, 99–111.

Gregg, M. C. 1976 Finestructure and microstructure observations during the passage of a mild storm. *J. phys. Oceanogr.* **6**, 528–555.

Kundu, P. J. 1976 An analysis of inertial oscillations observed near the Oregon Coast. *J. phys. Oceanogr.* **6**, 879–893.

Large, W. G. & Pond, S. 1982 Sensible and latent heat flux measurements over the ocean. *J. phys. Oceanogr.* **12**, 464–482.

MacVean, M. K. & Woods, J. D. 1980 Redistribution of scalars during upper ocean frontogenesis: a numerical model. *Q. Jl R. met. Soc.* **106**, 293–311.

Pollard, R. T. & Millard, R. C. 1970 Comparison between observed and simulated wind-generated inertial oscillations. *Deep-Sea Res.* **17**, 813–821.

Pollard, R. T. & Saunders, M. A. 1978*a* Navigation in the JASIN area during *Discovery* cruise 94. JASIN news, no. 10.

Pollard, R. T. & Saunders, P. M. 1978*b* Air–sea interaction: the structure of the upper ocean during JASIN 1978. R.R.S. *Discovery* cruise 94, cruise report no. 74, Institute of Oceanographic Sciences.

Pollard, R. T. 1980*a* Properties of near-surface inertial oscillations. *J. phys. Oceanogr.* **10**, 385–398.

Pollard, R. T. 1980*b* Calibration of IOS VACMs during JASIN 1978. JASIN news, no. 16.

Pollard, R. T. 1980*c* Reduction of JASIN batfish data. JASIN news, no. 17.

Pollard, R. T. 1982*a* Mesoscale (50–100 km) circulations revealed by inverse and classical analysis of the JASIN hydrographic data. *J. phys. Oceanogr.* (In the press.)

Pollard, R. T. 1982*b* Eddies and fronts in the JASIN area. JASIN news, no. 25.

Weller, R. A. 1982 The relation of near-inertial motions observed in the mixed-layer during the JASIN (1978) experiment to the local wind stress and to the quasigeostrophic flow field. *J. phys. Oceanogr.* **12**, 1122–1136.

PHILOSOPHICAL TRANSACTIONS OF THE ROYAL SOCIETY A MATHEMATICAL, PHYSICAL & ENGINEERING SCIENCES

PHILOSOPHICAL TRANSACTIONS OF THE ROYAL SOCIETY A MATHEMATICAL, PHYSICAL & ENGINEERING SCIENCES